Geophysical Research Letters

Supporting Information for

Melt onset over Arctic sea ice controlled by atmospheric moisture transport

Jonas Mortin[1], Gunilla Svensson[1*], Rune G. Graversen[2], Marie-Luise Kapsch[3], Julienne C. Stroeve[4,5], and Linette N. Boisvert[6]

[1]*Department of Meteorology and Bolin Centre for Climate Research, Stockholm University, 106 91 Stockholm, Sweden*

[2]*Department of Physics and Technology, UiT The Arctic University of Norway, 9019 Tromsø, Norway*

[3]*Max-Planck-Institute for Meteorology, Bundesstraße 53, 20146 Hamburg, Germany*

[4]*National Snow and Ice Data Center (NSIDC), Cooperative Institute for Research in Environmental Sciences (CIRES), University of Colorado, UCB 449, Boulder, CO 80309-0449, USA*

[5]*Centre for Polar Observation and Modelling, Earth Sciences/Department of Space & Climate Physics (MSSL), University College London, London, WC1E 6BT, UK*

[6]*Earth System Science Interdisciplinary Center (ESSIC), University of Maryland, 5825 University Research Ct #4001, College Park, MD 20740, USA*

*Corresponding author's email: gunilla@misu.su.se

Contents of this file

Introduction

This supporting information contains text and a number of figures to support the main document. First, Text S1 describes our view on the confidence of different ERA-Interim parameters in the context of this paper, and justifies which parameters are included in the main text and which are included in Figure S1. Second, most of the processing steps and the methodology are described in the main document. Here, Text S2 describes the additional processing steps necessary for Figures S1 – S3 in this supporting information.

Figure S1 shows the anomaly analysis applied to additional ERA-Interim fields, in order to give a more complete view of the atmospheric state around melt, while retaining space in the main document. Figure S1 supports our overall conclusions. Figure S2 shows how several atmospheric fields vary in the vertical around melt, to portrait a more complete view of the atmospheric state. Lastly, Figure S3 shows additional frames of three-day periods of Figure 2 in the main text, showing how the variability of melt onset corresponds to the variability of moist air masses.

Text S1.

Most of the analysis presented is based on ERA-Interim reanalysis products. Atmospheric reanalysis provides the best available observational constrained data available in the Arctic for which ERA-Interim is evaluated to be one of the best [*Lindsay et al.*, 2014]. However, in data-sparse regions such as over the Arctic sea-ice domain, the reanalysis solution is more dependent on the model structure, assumptions, and data-assimilation methods than in data-rich regions. For example, ERA-Interim underestimates the amount of liquid water present in clouds, thereby also underestimating LWD [*Engström et al., 2014*]; also skin temperatures and evaporation (i.e. latent heat flux) show large errors in ERA-Interim [Boisvert et al., 2015]. Further, the albedo of the sea-ice surface is largely based on climatological values in ERA-Interim and the sea ice lacks snow cover [*ECMWF*, 2013]. For these reasons, we choose to present our anomaly analysis of parameters not directly affected by surface processes in Figure 1 in the main text. Figure S1 provides additional parameters which we judge to be more uncertain (at varying degree), being more influenced by local model processes or the method with which they are obtained. Nevertheless, they support the overall conclusions.

Text S2.

The radiative and turbulent fluxes as well as precipitation and cloud water are 24-h forecasts initiated at 00 UTC; other fields are daily means of 6-hourly analyses. The atmospheric latent-heat transport and the dry static energy transport are vertically integrated on model hybrid levels from the top to the bottom of the atmosphere [*Graversen*, 2006]. A barotropic mass correction is applied to the flux [*Trenberth*, 1991]. They are based on ERA-Interim data with a spatial resolution of 0.5° x 0.5° for the period 1979 – 2012. The transport convergence of the latent heat and dry-static energy is defined as

$$J_{\mathrm{latent}} = \nabla \frac{1}{g} \int_0^1 \mathbf{v} L q \frac{\partial p}{\partial \eta} \mathrm{d}\eta$$

$$J_{\mathrm{dry}} = \nabla \frac{1}{g} \int_0^1 \mathbf{v} (0.5\mathbf{v} \cdot \mathbf{v} + c_p T + gz) \frac{\partial p}{\partial \eta} \mathrm{d}\eta$$

respectively, where g is gravity, $\boldsymbol{v}$ is the horizontal wind vector, p is pressure, L is the specific heat of condensation, q is the specific humidity, c_p is the specific heat capacity of moist air at constant pressure, T is temperature, g is the gravity, and is the vertical hybrid coordinate used in ERA-Interim.

The method to include and exclude data for Figure S2 is the same as for Figure 1 in the main text. That is, the number of data points (at a given vertical level) is the same as in the anomaly analysis for Figure 1 in the main text, but with another categorization of the melt data.

References Text S1 to S2.

ECMWF (2013), *IFS Documentation, Cy38r1, Part IV: Physical Processes*, Shinfield Park, Reading, England. [online] Available from: http://ecmwf.int/research/ifsdocs

Boisvert, L. N., D. L. Wu, T. Vihma, and J. Susskind (2015), Verification of air/surface humidity differences from AIRS and ERA-Interim in support of turbulent flux estimation in the Arctic, *J. Geophys. Res. Atmos.*, 120, doi:10.1002/2014JD021666.

Engström, A., J. Karlsson, and G. Svensson (2014), The Importance of Representing Mixed-Phase Clouds for Simulating Distinctive Atmospheric States in the Arctic, *J. Clim., 27*(1), 265-272, doi: 10.1175/JCLI-D-13-00271.1.

Graversen, R. G. (2006), Do Changes in the Midlatitude Circulation Have Any Impact on the Arctic Surface Air Temperature Trend?, *J. Clim.*, *19*(20), 5422–5438, doi:10.1175/JCLI3906.1.

Lindsay, R., M. Wensnahan, A. Schweiger, and J. Zhang (2014), Evaluation of Seven Different Atmospheric Reanalysis Products in the Arctic, *J. Clim.*, *27*(7), 2588–2606, doi:10.1175/JCLI-D-13-00014.1.

Trenberth, K. E. (1991), Climate Diagnostics from Global Analyses: Conservation of Mass in ECMWF Analyses, *J. Clim.*, *4*(7), 707–722, doi:10.1175/1520-0442(1991)004<0707:CDFGAC>2.0.CO;2.

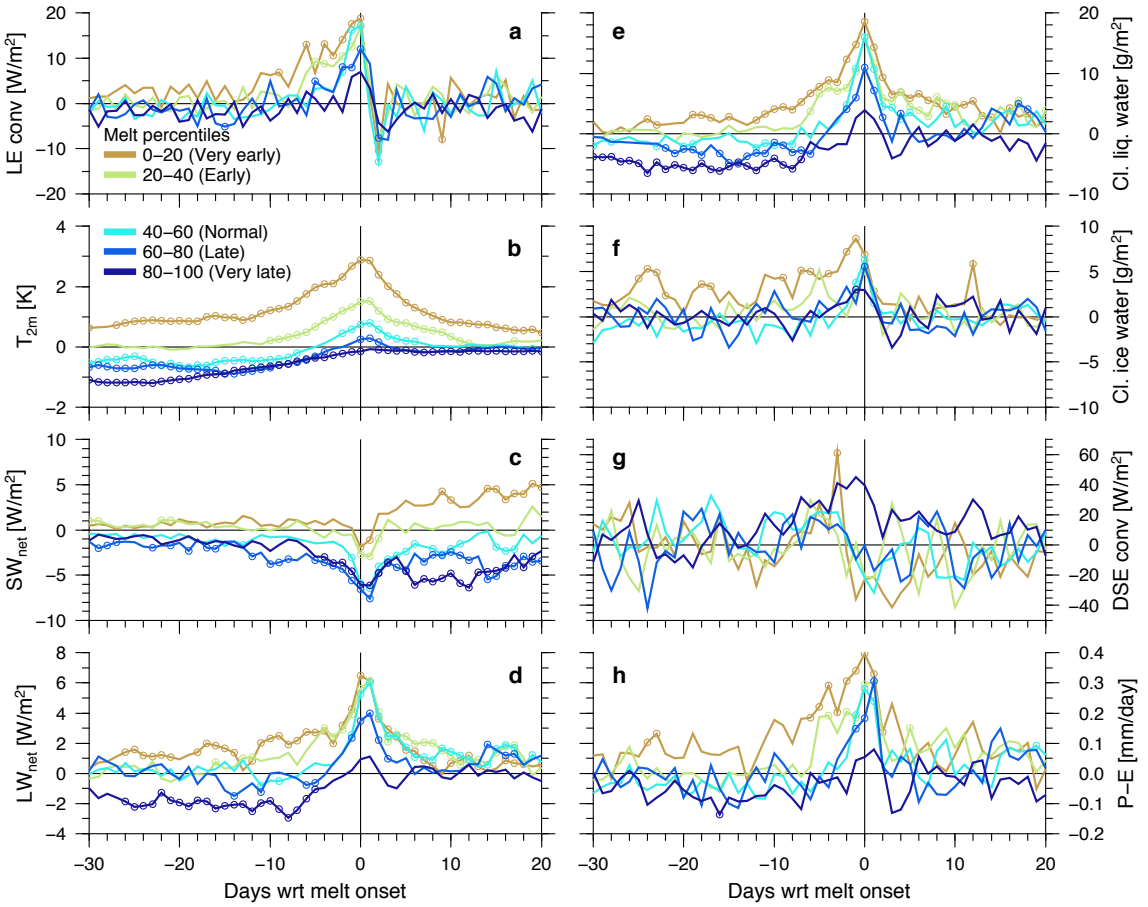

Figure S1. Anomaly composites of atmospheric fields relative to the local melt onset in five categories. Like Figure 1 in the main text, but for (a), latent heat transport convergence (proportional to the moisture-transport convergence), (b), 2-meter temperature, (c), Surface net shortwave radiation, (d), surface net longwave radiation, (e), Total column cloud liquid water, (f), total column cloud ice water, (g), dry-static energy transport convergence, (h), precipitation minus evaporation in unit of mm water equivalent per day, defined as positive downward. Dots in (c)–(h) indicate statistical significance ($p \leq 0.01$). Data in all panels are from ERA-Interim. See Text S2 on how transport convergences are calculated.

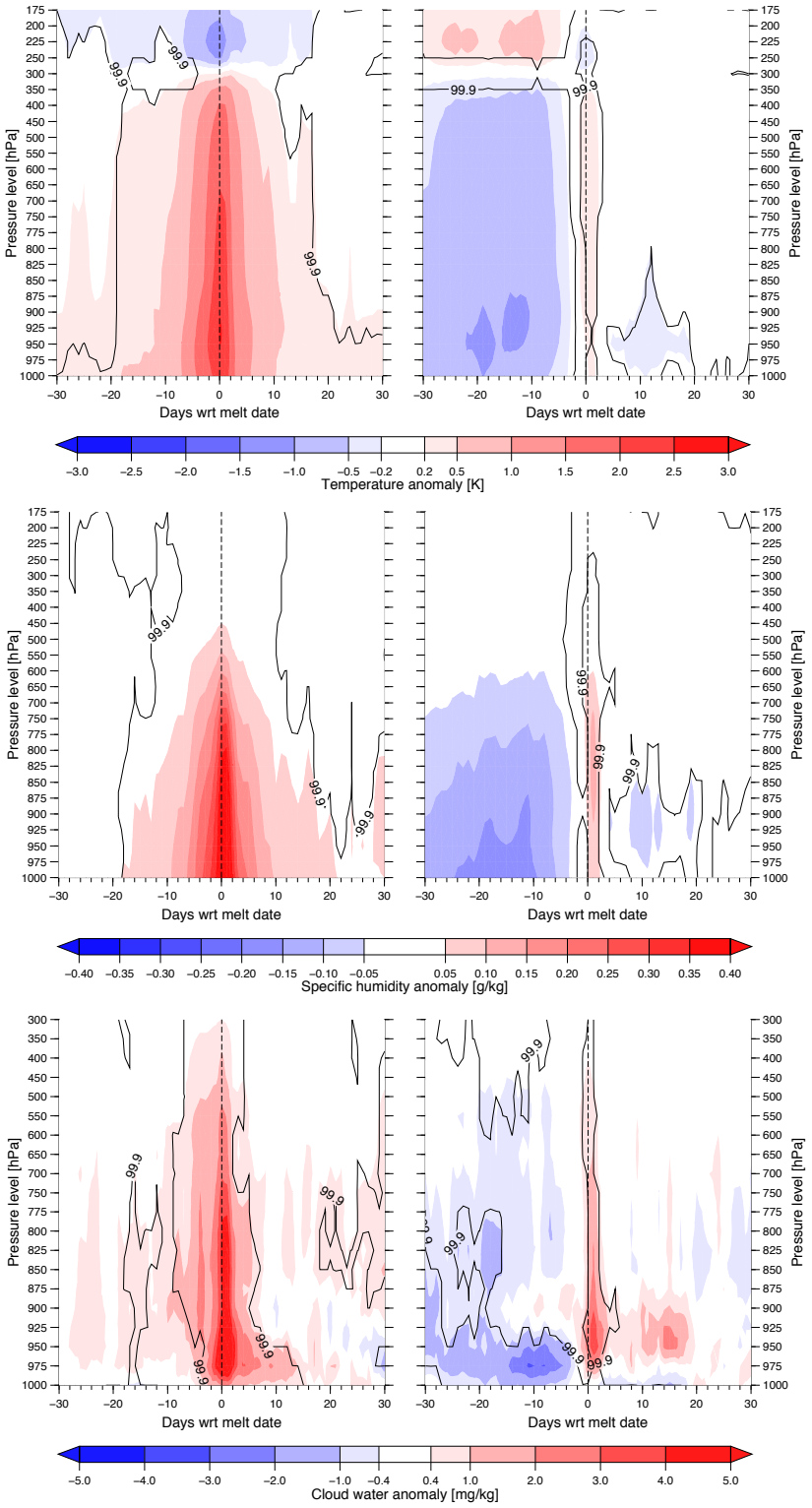

Figure S2. Vertical profiles of temperature, moisture, and cloud-water anomalies for an early (left column) and a late (right column) melt onset. Anomalies are relative to the climatology and are temporally displaced with regard to the melt date (as in Figure 1 in the main text). Black contours show the significance at the 99.9% confidence level (see Section 2 in the main text). All data are from ERA-Interim.

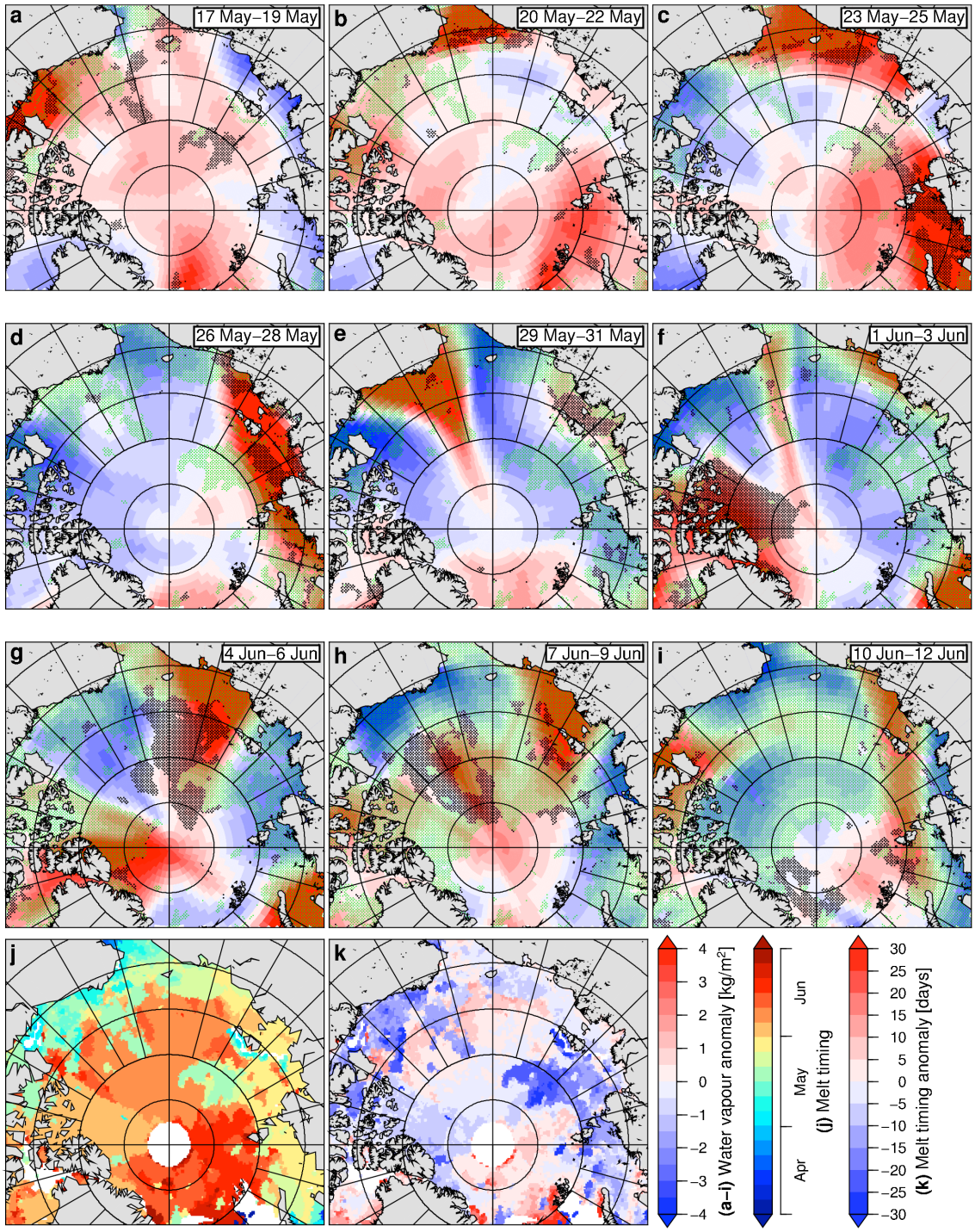

Figure S3. Example of melt onset and water-vapor anomalies. As Figure 2 in the main text, but with additional frames for additional three-day periods.

Table S1. Trends of early melt onset dates between 1979 and 2016. The regions are defined in *Stroeve et al. [2014]*.

Region	**Early Melt Onset Trends** [days/decade]
Arctic Region	-2.6*
Barents Sea	-8.3*
Greenland Sea	-7.8*
Baffin Bay	-5.3*
Kara Sea	-5.1*
Hudson Bay	-3.3*
Beaufort Sea	-2.8*
Chukchi Sea	-2.2
Laptev Sea	-2.2
Central Arctic	-1.66*
Canadian Archipelago	-1.45
East Siberian Sea	-1.26
Sea of Okhotsk	-0.6
Bering Sea	0.84

*Statistically significant trends.